

# Cation distribution and infrared properties of $\text{Ni}_x\text{Mn}_{1-x}\text{Fe}_2\text{O}_4$ ferrites

QIANG-MIN WEI\*, JIAN-BIAO LI, YONG-JUN CHEN

State Key Laboratory of New Ceramics and Fine Processing, Department of Materials Science and Engineering, Tsinghua University, Beijing, 100084, People's Republic of China  
E-mail: wqm99@mails.tsinghua.edu.cn

The spinel ferrite system  $\text{Ni}_x\text{Mn}_{1-x}\text{Fe}_2\text{O}_4$ , with  $x = 0, 0.1, 0.25, 0.5, 0.75$  and  $1$ , is prepared by the standard double sintering ceramic method. X-ray diffraction and IR spectroscopy are used to analyze the relationship between infrared properties and content of the nickel ions. With nickel ion substitution addition, the lattice parameter, X-ray density, cation distribution, inversion parameter and radius of octahedral and tetrahedral sites are calculated. The IR spectra obtained at room temperature in the frequency range  $350\text{--}1000\text{ cm}^{-1}$ , show four absorption bands. The high frequency band ( $\nu_1$ ) and low frequency band ( $\nu_2$ ) are assigned to the tetrahedral and octahedral complexes, respectively. The relationship between bands and nickel content was also investigated and found that the absorption bands linearly increase with the increasing content of nickel ions, which is correlated to the cation distribution calculated by Bertaut method. © 2001 Kluwer Academic Publishers

## 1. Introduction

The magnetic and electrical properties of the spinel ferrites are strongly dependent on their physical structure, known by the general formula  $\text{AB}_2\text{O}_4$ , consisting of an almost perfect interstices cubic closed-packed oxygen arrangement, in which the cations reside on tetrahedral and octahedral intersites. The unit cell is obtained by doubling the approximately face-centered cubic oxygen sublattice along each of three directions. Of the resulting 64 tetrahedral or (A) sites and 32 octahedral or (B) sites, only 8 and 16 are occupied, respectively, by cations in stoichiometric spinel. The majority of spinel compounds belong to the space group  $Fd\bar{3}m(F_{1/d}^4\bar{3}_2/m, \text{No.227}$  in the International Tables) [1] and lattice parameter is typically  $\sim 8.5\text{ \AA}$ . Occupation of the tetrahedral site entirely with a divalent transition metal produces a normal spinel structure, while occupation of the octahedral site with the divalent transition metal yields an inverse spinel structure. If divalent transition-metal ions are present on both A and B sublattices, the structure is mixed or disordered. Determination of cation distribution at the tetrahedral and octahedral sites has thus been a subject of many studies.

Extensive investigations of manganese ferrites have been reported giving useful information about the influence of divalent Cu [2], Zn [3] and trivalent Co [4–6], Cr [7] substitutions in  $\text{MnFe}_2\text{O}_4$  on various properties. Most of these studies, however, pay less attention to nickel substituted manganese ferrite except Mössbauer measurement [4].

Cation distribution in  $\text{MnFe}_2\text{O}_4$  and  $\text{NiFe}_2\text{O}_4$  has been determined using neutron diffraction and

Mössbauer methods, which confirmed that cation distribution in  $\text{NiMn}_2\text{O}_4$  is the random arrangement and  $\text{NiFe}_2\text{O}_4$  is an inverse spinel [4].

In the present studies, the cation distribution in tetrahedral and octahedral sites and the infrared spectra are obtained using XRD and IR spectra on the mixed spinel  $\text{Ni}_x\text{Mn}_{1-x}\text{Fe}_2\text{O}_4$  with  $X$  from 0.0 to 1.0. The relationship between absorption band and cation distribution is also established.

## 2. Experimental procedure

The samples are prepared, in polycrystalline form, by conventional double sintering ceramic technique. Proportional amounts of  $\text{Fe}_2\text{O}_3$ , NiO and MnO are mixed thoroughly, pelleted and then fired at  $1200^\circ\text{C}$  for 6 hours in the air. After furnace cooling, the materials were ground, repelletized, fired again at  $1250^\circ\text{C}$  in the air for 20 hours and then quenched to room temperature. With this rising calcining technology, the amount of  $\text{Mn}^{3+}$  in the ferrite systems becomes negligible [8].

Lattice parameters and diffraction intensities are obtained using a Rigaku-D/max-IIIb X-ray diffractometer equipped with a graphite crystal monochromator and scintillation counter.  $\text{Fe-K}\alpha$  radiation is used in all cases. Prolonged grinding of samples and back loading of the specimen holder were performed in order to minimize preferred orientation effects. Diffraction pattern is scanned at a speed of  $0.120^\circ\text{ min}^{-1}$  ( $2\theta$ ). By counting the intensity at each side of the diffraction line over a time interval which is long enough such that the background is determined with a negligible statistical error [9].

\* Author to whom all correspondence should be addressed.

The IR spectra in the range from 350 to 1000  $\text{cm}^{-1}$  are recorded at room temperature using the infrared spectrometer model SPECTRUM-GX.

### 3. Results and discussion

#### 3.1. X-ray analysis

X-ray diffraction patterns of  $\text{Ni}_x\text{Mn}_{1-x}\text{Fe}_2\text{O}_4$  (with  $x = 0, 0.25, 0.50, 0.75$  and 1) are shown in Fig. 1. These diffraction lines corresponding to a cubic, spinel-type and crystalline phase provide clear evidence of the formation of a series of solid solutions between  $\text{NiFe}_2\text{O}$  and  $\text{MnFe}_2\text{O}$ . The values of the lattice parameter,  $a$ , exhibit a linear content dependence, thus obeying Vegard's law [10] as shown in Fig. 2. Since the ionic radius of  $\text{Ni}^{2+}$  (Tet.: 0.55 Å; Oct.: 0.69 Å) is smaller than that of  $\text{Mn}^{2+}$  (Tet: 0.655Å; Oct: 0.80 Å) [11], the replacement of manganese by nickel ions leads to a decrease of the lattice parameter. The X-ray density  $D_x$  calculated using the formula  $D_x = 8M/Na$ , where  $M$  is the molecular weight,  $N$  Avogadro's number and  $a$  the lattice parameter, increases linearly with the increasing nickel content as shown in Fig. 3. Moreover, the Ni

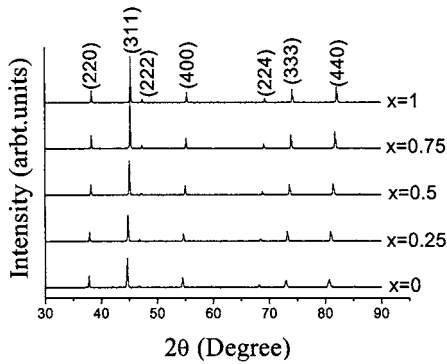


Figure 1 X-ray diffraction patterns of  $\text{Ni}_x\text{Mn}_{1-x}\text{Fe}_2\text{O}_4$  ferrites.

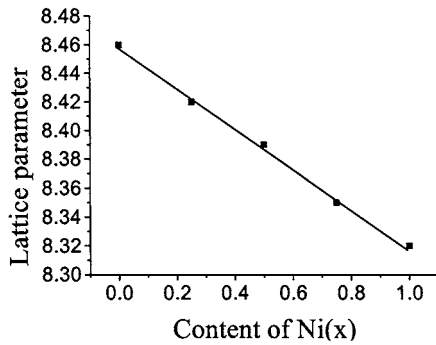


Figure 2 Lattice parameter as a function of the  $\text{Ni}^{2+}$  content.

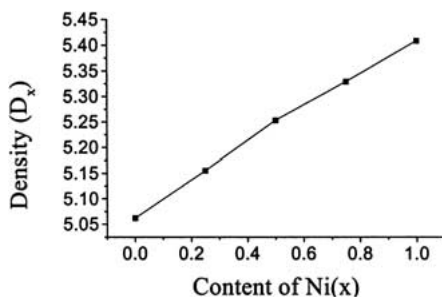


Figure 3 Variation of X-ray density with  $\text{Ni}^{2+}$  content.

atom is heavier than Mn, and this increase in weight and decrease in size cause an increase in the X-ray density.

The values of lattice parameter found for  $\text{NiFe}_2\text{O}_4$  ( $a = 8.320$  Å) and  $\text{MnFe}_2\text{O}_4$  ( $a = 8.449$  Å) agree with those reported by several authors [8, 11, 12].

The cation distribution in spinel ferrite can be obtained from the analysis of X-ray diffraction. The Bertaut [13], Furuhashi *et al.* [14], and  $R$ -factor [13] are all based on a comparison between the diffraction intensities observed experimentally and those calculated for a large number of hypothetical crystal structures. Additionally, thermoelectric method [15, 16], Neutron diffractometry [17], nuclear magnetic resonance [1], and electron spin resonance [18] are also used to study cation distribution.

In the present paper, the Bertaut method is used to determine the cation distribution. This method selects a few pairs of reflections according to expression (1)

$$I_{hkl}^{\text{obs.}} / I_{h'k'l'}^{\text{obs.}} = I_{hkl}^{\text{calc.}} / I_{h'k'l'}^{\text{calc.}} \quad (1)$$

where  $I_{hkl}^{\text{obs.}}$  and  $I_{hkl}^{\text{calc.}}$  are the observed and calculated intensities for reflection  $hkl$  respectively. If an agreement factor,  $R$ , is defined as in the following Equation 2, the simulated structure which best matches the actual structure of the sample will lead to a minimum value of  $R$ . Corresponding cation distribution is obtained for each  $hkl$ ,  $h'k'l'$  reflection pair considered.

$$R = |(I_{hkl}^{\text{obs.}} / I_{h'k'l'}^{\text{obs.}}) - (I_{hkl}^{\text{calc.}} / I_{h'k'l'}^{\text{calc.}})| \quad (2)$$

In this method, the value of the agreement factor,  $R$ , (in this paper,  $R < 0.05$ ) is the indicator of the reliability of the results. The best information on cation distribution is achieved when comparing experimental and calculated intensity ratios for reflections whose intensities (i) are nearly independent of the oxygen parameter, (ii) vary with the cation distribution in opposite ways, and (iii) do not differ significantly. The most suitable reflections are (220), (400), and (422). Besides, a value of oxygen parameter ( $u$ ) has to be assumed for the determination of  $I_{hkl}^{\text{calc.}}$ . Table I shows the values of oxygen parameter ( $u$ ) and the cation distribution parameter.

For a given spinel compound, the anion sublattice expands or contracts on varying oxygen parameter ( $u$ ) until the A and B site volumes match the radii of the constituent cations. The previously reported values of the oxygen parameter for  $\text{NiFe}_2\text{O}_4$  and  $\text{MnFe}_2\text{O}_4$ [11] are entirely consistent with the results calculated in present study.

TABLE I Oxygen parameter,  $u$ , and cation distribution for  $\text{Ni}_x\text{Mn}_{1-x}\text{Fe}_2\text{O}_4$  spinel

$x$	$u$	Tetrahedral			Octahedral		
		$\text{Ni}^{2+}$	$\text{Mn}^{2+}$	$\text{Fe}^{3+}$	$\text{Ni}^{2+}$	$\text{Mn}^{2+}$	$\text{Fe}^{3+}$
0	0.386	–	0.80	0.200	–	0.20	1.8
0.25	0.384	0.007	0.65	0.343	0.243	0.10	1.657
0.5	0.383	0.015	0.43	0.555	0.485	0.07	1.445
0.75	0.383	0.091	0.18	0.729	0.659	0.07	1.271
1	0.382	0.001	–	0.999	0.999	–	1.001

TABLE II Cation-anion distance in  $\text{Ni}_x\text{Mn}_{1-x}\text{Fe}_2\text{O}_4$  ferrite

$x$	$u$	Tet edge	Octa edge		Tet bond	Oct bond
			Shared	Unshared		
0.0	0.386	3.247	2.722	2.99	1.988	2.022
0.25	0.384	3.188	2.760	2.977	1.952	2.030
0.50	0.383	3.153	2.774	2.966	1.931	2.030
0.75	0.383	3.141	2.763	2.956	1.923	2.025
1	0.382	3.110	2.781	2.948	1.915	2.026

Using the experimental values of lattice and oxygen position parameters and following equations given in Equations 3–7 [3], the interionic distances and the radii of the tetrahedral and octahedral bonds are calculated and shown in Table II.

$$d_{\text{AX}} = \sqrt{3}\left(u - \frac{1}{4}\right)a \quad (\text{tet. Bond}) \quad (3)$$

$$d_{\text{BX}} = \left(3u^2 - \frac{11u}{4} + \frac{43}{64}\right)^{\frac{1}{2}} a \quad (\text{oct. bond}) \quad (4)$$

$$d_{\text{XX}} = \sqrt{2}\left(2u - \frac{1}{2}\right)a \quad (\text{tet. edge}) \quad (5)$$

$$d_{\text{XX}} = \sqrt{2}(1 - 2u)a \quad (\text{shared oct. edge}) \quad (6)$$

$$d_{\text{XX}} = \left(4u^2 - 3u + \frac{11}{16}\right)^{\frac{1}{2}} a \quad (\text{unshared oct. edge}) \quad (7)$$

Inversion parameter,  $\gamma$ , defined as the total fraction of divalent ions lodged in octahedral sites, can be calculated from the data given in Table I. The degree of inversion vs. Ni content ( $x$ ) is shown in Fig. 4. It is seen that  $\gamma$  increases linearly from 0.2 up to 0.99 at the end of the solid solution series.  $\text{Ni}^{2+}$  is well known to occupy exclusively octahedral sites because of its large octahedral site preference energy. Table I shows, however, that considerable amount of  $\text{Ni}^{2+}$  ions is added to the

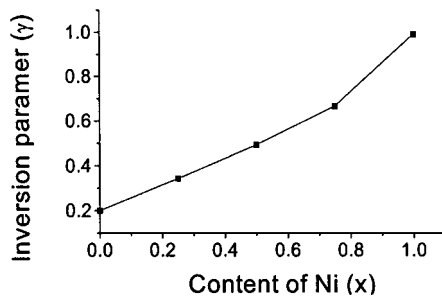


Figure 4 The degree of inversion vs. Ni content ( $x$ ).

TABLE III IR absorption bands of  $\text{Ni}_x\text{Mn}_{1-x}\text{Fe}_2\text{O}_4$

Sites	Bands	$\text{Ni}_x\text{Mn}_{1-x}\text{Fe}_2\text{O}_4$					Me- $\text{O}^{2-}$
		$X = 0$	$X = 0.25$	$X = 0.5$	$X = 0.75$	$X = 1$	
Tetrahedral	$\nu_1$	551	563	574	582	591	$\text{Fe}^{3+}\text{O}^{2-}$
	$\nu_1$	482	750	-	750	-	$\text{Mn}^{2+}\text{-O}^{2-}$
Octahedral	$\nu_2$	373	373	373	373	373	$\text{Fe}^{3+}\text{-O}^{2-}$
	$\nu_2$	-	460	466	465	465	$\text{Ni}^{2+}\text{-O}^{2-}$

tetrahedral sites with the increasing content of the  $\text{Mn}^{2+}$  ions. These results confirm that in mixed spinel structure the individual site preference of any two cations can be significantly affected by the third ones, which has also been studied in previous works [5, 19].

### 3.2. IR spectra

The IR spectra for the system  $\text{Ni}_x\text{Mn}_{1-x}\text{Fe}_2\text{O}_4$  ferrites are recorded in the range from 350 to 1000  $\text{cm}^{-1}$  as shown in Fig. 5. The spectra indicate the presence of four absorption bands,  $\nu_1$ ,  $\nu_1'$ ,  $\nu_2$ , and  $\nu_2'$  in the range from 350 to 700  $\text{cm}^{-1}$ , which is the common feature of all spinel structure. The band  $\nu_1$  is attributed to the stretching vibration of  $\text{Fe}^{3+}\text{-O}^{2-}$  in the tetrahedral complexes and the  $\nu_2$  to that of octahedral complexes [20, 21]. The two low-frequency bands  $\nu_1'$  and  $\nu_2'$  are attributed to some type of lattice vibration. The values of the absorption band frequency are given in Table III. The position and intensities of  $\nu_1$  and  $\nu_2$ , due to the difference in the  $\text{Fe}^{3+}\text{-O}^{2-}$  distances for the tetrahedral and octahedral sites, change slightly with  $x$ . Variation of the primary bands  $\nu_1$ ,  $\nu_2$  with the composition ( $x$ ) is shown in Fig. 6. It is seen that the absorption band  $\nu_2$  linearly increases with the increasing content of nickel ions while band  $\nu_1$  remains constant. The cation distribution given in Table I shows that the  $\text{Ni}^{2+}$  ions entirely occupy the octahedral sites and force the  $\text{Fe}^{3+}$  ions into tetrahedral sites with the increasing nickel ions. Therefore, because the radius of  $\text{Mn}^{2+}$  (Tet.: 0.655 Å;) is larger than that of  $\text{Fe}^{3+}$  (Tet.: 0.49 Å;) while the  $\text{Ni}^{2+}$  (Oct.: 0.69 Å) is about the same as the  $\text{Fe}^{3+}$  (Oct.: 0.66 Å) [11], the radius of tetrahedral becomes larger and that of octahedral hardly change with the content of the  $\text{Ni}^{2+}$  ions as represented in Table II. This may be one of the reasons for explaining the variance of bands  $\nu_1$  and  $\nu_2$ .

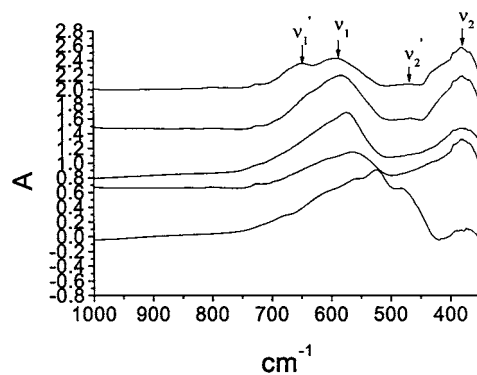


Figure 5 The IR spectra of  $\text{Ni}_x\text{Mn}_{1-x}\text{Fe}_2\text{O}_4$ .

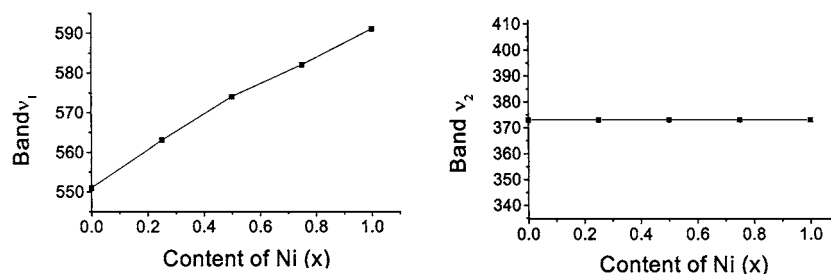


Figure 6 Variation of the primary band  $\nu_1$  and  $\nu_2$  with the composition ( $x$ ) of  $\text{Ni}_x\text{Mn}_{1-x}\text{Fe}_2\text{O}_4$ .

The presence of divalent ions on tetrahedral sites would explain the existence of the weak band  $\nu'_1$ . It is known that the  $\text{Mn}^{2+}$  ions occupy mainly the tetrahedral sites (A sites), as shown in X-ray studies. Accordingly, this shoulder can be attributed to the vibration of  $\text{Mn}^{2+}-\text{O}^{2-}$  in tetrahedral complexes.

On the octahedral sites (B sites), the small band at  $\nu'_2 \approx 465$ , due to the presence of large fraction of  $\text{Ni}^{2+}$  ions in the octahedral sites, can be assigned to the  $\text{Ni}^{2+}-\text{O}^{2-}$  octahedral complexes as shown in Table III. On the basis of the above analysis, the cation distribution for  $\text{Ni}_x\text{Mn}_{1-x}\text{Fe}_2\text{O}_4$  can be determined as followings:



where,  $\gamma$  is the inversion parameter,  $\alpha$  is the fraction of tetrahedral sites occupied by nickel ions, A and B denote the tetrahedral and octahedral sites respectively. The results are fairly well agreement with the calculation using X-ray diffraction.

#### 4. Conclusions

The distribution of cation in  $\text{Ni}_x\text{Mn}_{1-x}\text{Fe}_2\text{O}_4$  systems using XRD has revealed that these systems belong to the family of mixed or partially inverse spinel ferrites. The IR spectra show two fundamental bands  $\nu_1$  and  $\nu_2$  in the frequency range  $350-1000\text{ cm}^{-1}$ , corresponding to the tetrahedral and octahedral complexes, respectively. The band  $\nu_1$  shifts towards the high-frequency side while the band  $\nu_2$  remains constant with increasing nickel ions, which can be attributed to the cation distribution calculated by X-ray diffraction.

#### Acknowledgement

The authors thank Xiao-jun Guo for performing X-ray measurements.

#### References

1. K. E. SICKAFUS and J. M. WILLS, *J. Amer. Ceram. Soc.* **82** (12) (1999) 3297.
2. M. U. RANA, M.-U. ISLAM and T. ABBAS, *Mater. Lett.* **41** (1999) 52.
3. T. ABBAS, Y. KHAN, M. AHMAD and S. ANWAR, *Solid State Commun.* **82**(9) (1992) 701.
4. V. K. SINGH, N. K. KHATRI and S. LOKANATHAN, *Pramana* **16**(4) (1981) 273.
5. D. C. CARTER and T. O. MASON, *J. Amer. Ceram. Soc.* **71**(4) (1988) 213.
6. M. K. FAYEK, F. M. SAYEDAHMED and S. S. ATALLAH, *J. Mater. Sci.* **27** (1992) 4813.
7. M. N. KHAN and A. AHMED, *ibid.* **24** (1989) 2615.
8. M. A. AMER, *Phys. Stat. Sol. (A)* **151** (1995) 205.
9. C. O. AREAN, J. S. D. VINUELA, J. M. R. GONZALEZ and A. M. ARJONA, *Mater. Chem.* **6** (1981) 165.
10. B. D. CULLITY, "Elements of X-ray Diffraction" (Addison Wesley Publishing Reading, MA, 1956) p. 352.
11. HUGH ST. C. O'NEILL and A. NAVEOTSKY, *Am. Miner.* **68** (1983) 181.
12. M. EL GELNPOUZL, K. SBAL, P. PIRRIOL and B. ASABRAIL, *Mater. Chem. Phys.* **25** (1990) 429.
13. J. M. R. GONZALEZ and C. O. AREAN, *J. Chem. Soc. Dalton Trans.* (1985) 2155.
14. H. FURUHASHI, M. INAGAKI and S. NAKA, *J. Inorg. Chem.* **35** (1973) 3009.
15. C. C. WU and T. O. MASON, *J. Amer. Ceram. Soc.* **64**(9) (1981) 520.
16. C. C. WU, S. KUMARAKRISHAN and T. O. MASON, *J. Solid State Chem.* **37**(2) (1981) 144.
17. E. STALL, P. FISCHER, W. HALG and G. MAIER, *J. Phys. Paris.* **25** (1964) 447.
18. U. SCHMOCKER, H. R. BOESCH and F. WALDNER, *Phys. Lett.* **40A**(3) (1972) 237.
19. P. PORTA, F. S. STONE and R. G. TUNER, *J. Solid State Chem.* **11** (1974) 135.
20. O. S. JOSYULU and J. SOONLANADRL, *Phys. State Sol. (A)* **65** (1981) 479.
21. M. A. AMER, *ibid.* **145** (1994) 157.

Received 17 November 2000  
and accepted 23 July 2001